Journal of Engineering Sciences and Innovation
Volume 2, Issue 1 / 2017, pp. 1-12

Technical Sciences
Academy of Romania
www.jesi.astr.ro

A. Mechanics, Mechanical and Industrial Engineering, Mechatronics

Received ***8 November 2016*** *Accepted* ***5 March 2017***
Received in revised from ***15 January 2017***

On the bloch boundary conditions in sonic composites

VETURIA CHIROIU[*1], **IULIAN GIRIP**[1], **LIGIA MUNTEANU**[1], **POLIDOR BRATU**[2]

[1]*Institute of Solid Mechanics, Romanian Academy, Bucharest, Romania*
[2]*Research Institute for Construction Equipment and Technology-ICECON, Bucharest, Romania*

Abstract. A sonic composite is a finite size periodic array composed of scatterers embedded in a homogeneous material which has the unique property of exhibiting the band-gaps, where the sound is not allowed to propagate due to complete reflections. We propose in this paper an inverse problem to calculate the band structure of a sonic plate, based on evanescent Bloch boundary conditions between the scatterrers and the matrix, and the cnoidal superposition of waves. The sonic plate is composed of an array of acoustic scatterers embedded into an epoxy matrix. The scatterers are piezoceramic hollow spheres made from functionally graded materials with radial polarization, which support the Reddy and cosine laws. The proposed method requires the displacements registered at both sides of the plate. This allows the band structures to be determined experimentally. The Bloch boundary conditions greatly reduces the computational effort because they cancels the necessity to introduce non-reflecting boundary condition at the ends of the plate if sharp periodic boundary conditions between the scatterers and the matrix are used.

Keywords: sonic composite, Bloch boundary conditions, band-gaps, acoustic scatterer.

1. Introduction

The band-gaps or Bragg reflections occur at different frequencies inverse proportional to the central distance between two scatterers of a sonic composite. A sonic composite is a finite size periodic array composed of scatterers embedded in

[*] Corresponding author: Veturia Chiroiu, C-tin Mille 15, Bucharest 010141
email: veturiachiroiuilie@gmail.com

a homogeneous material which has the property of exhibiting the frequency band-gaps where the sound is not allowed to propagate 1–7].

Due to their unique properties, sonic composites have great potential in many applications, including vibration and sound isolation, acoustic cloaking and waveguiding. The evanescent field of waves is distributed across the boundary of the waveguide into the surrounding composite by several times the lattice constant, just like the evanescent field in the case of total reflection on the dielectric boundary [8-12].

The existence of a pronounced sound attenuation band connected to a large acoustic impedance ratio of the materials representing the matrix and scatterers is reported not only by experimental works [13-15], but also by theoretical works [16-18]. Liu *et al.* [19] built a sonic crystal consisting of an array of acoustic scatterers, which exhibit resonance frequencies themselves. These local resonators are silicone rubber coated metal spheres.

The sound attenuating frequency bands are not determined by the distribution of scatterers, but by their intrinsic structure. Hirsekorn *et al.* [20] have analyzed the sound attenuation of a sonic material consisting of an array of silicone rubber coated hollow steel cylinders embedded in an epoxy matrix. The results gain a better insight of the mechanisms governing local resonances that can be used to predict the structural parameters needed to fabricate custom-tailored sonic materials.

The primary goal of this paper is to propose an inverse problem based on evanescent Bloch boundary conditions and cnoidal superposition of waves to calculate the band structure of a sonic plate when damping is present. The method needs the displacements registered at both sides of the plate in a small number of points. The damping coefficient is obtained from the ratio of the displacements at the receiver and at the input transducer. This allows the band structures to be determined experimentally. The scatterers are made from functionally graded materials with radial polarization, which support the Reddy and cosine laws [21-23].

2. The sonic composite

The sonic composite is consisting of an array of acoustic scatterers embedded in an epoxy matrix. The acoustic scatterers are hollow spheres made from a nonlinear isotropic piezoelectric ceramic, while the matrix is made from a nonlinear isotropic epoxy resin (Fig. 1). The sonic plate consists of 72 local resonators of diameter a. A rectangular coordinate system $Ox_1x_2x_3$ is employed. The origin of the coordinate system $Ox_1x_2x_3$ is located at the left end, in the middle plane of the sample, with the axis Ox_1 in-plane and normal to the layers and the axis Ox_3 out-plane and normal to the plate. The length of the plate is l, its width is d, while the diameter of the hollow sphere is a and its thickness is $e > a$. In order to avoid unphysical reflections from the boundaries of the specimen, we have implemented

the absorbing boundary conditions in the x_1-direction, at $x_1 = 0$ and $x_1 = l$. A transducer and a receiver are located at $x_1 = b$ and $x_1 = l - b$, respectively. The role of the transducer is to inject into the plate the plane monochromatic waves propagating in the x_1-direction.

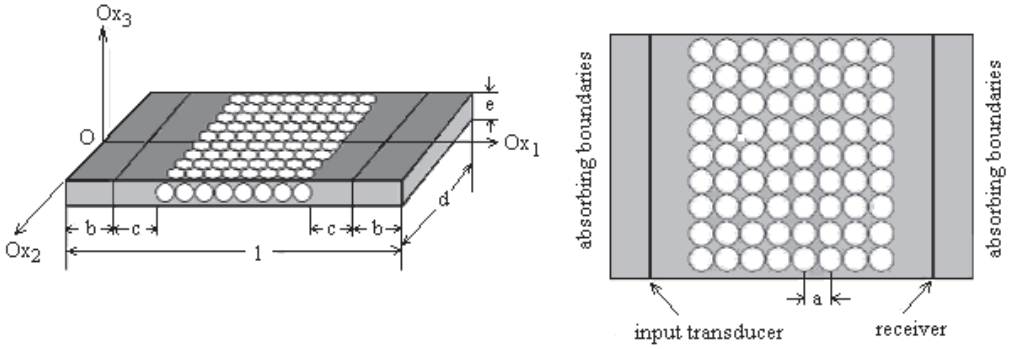

Fig. 1. Sketch of the sonic plate.

The basic equations of 3D spherically isotropic piezoelasticity for a sphere are given in [3, 25]. The center of anisotropy is the same with the origin of the spherical coordinate system (r, θ, φ). An index followed by a comma represents partial differentiation with respect to space variables, while a superposed dot indicates differentiation with respect to time. Throughout the paper, repeated indices denote summation over the range (1, 2, 3). The constitutive equations for the piezoelectric hollow sphere are given by

$$\Sigma_{\theta\theta} = r\sigma_{\theta\theta} = C_{11}S_{\theta\theta} + C_{12}S_{\varphi\varphi} + C_{13}S_{rr} + f_{31}r\phi_{r},$$

$$\Sigma_{\varphi\varphi} = r\sigma_{\varphi\varphi} = C_{12}S_{\theta\theta} + C_{11}S_{\varphi\varphi} + C_{13}S_{rr} + f_{31}r\phi_{,r},$$

$$\Sigma_{rr} = r\sigma_{rr} = C_{13}S_{\theta\theta} + C_{13}S_{\varphi\varphi} + C_{33}S_{rr} + f_{33}r\phi_{,r},$$

$$\Sigma_{r\theta} = r\sigma_{r\theta} = 2C_{44}S_{r\theta} + f_{15}\phi_{,\theta}, \quad \Sigma_{r\varphi} = r\sigma_{r\varphi} = 2C_{44}S_{r\varphi} + f_{15}\csc\theta\phi_{,\varphi}, \tag{1}$$

$$n_\tau = t_\tau / T_\tau, \tag{2}$$

$$\Sigma_{\theta\varphi} = r\sigma_{\theta\varphi} = 2C_{66}S_{\theta\varphi}, \quad \Lambda_\theta = rD_\theta = 2C_{15}S_{r\theta} - \zeta_{11}\phi_{,\theta},$$

$$\Lambda_\varphi = rD_\varphi = 2f_{15}S_{r\varphi} - \zeta_{11}\csc\theta\phi_{,\varphi}, \quad \Lambda_r = rD_r = f_{31}S_{\theta\theta} + f_{31}S_{\varphi\varphi} + f_{33}S_{rr} - \zeta_{33}r\phi_{,r},$$

where σ_{ij} is the stress tensor, ϕ is the electric potential, D_i is the electric displacement vector, C_{ij} are the elastic constants, $C_{66} = (C_{11} - C_{12})/2$, f_{ij} are the piezoelectric constants f_{ij}, ζ_{ij} are the dielectric constants, and $i = r, \theta, \varphi$. The elastic, piezoelectric and dielectric constants are arbitrary functions of the radial coordinate r. On denoting the components of the strain tensor and displacement

vector by ε_{ij} and u_i, $i=r,\theta,\varphi$, respectively, the quantities S_{ij} related to the strain tensor ε_{ij} are defined as

$$\begin{gathered} S_{rr}=r\varepsilon_{rr}=ru_{r,r}, \quad S_{\theta\theta}=r\varepsilon_{\theta\theta}=u_{\theta,\theta}+u_r, \\ S_{\varphi\varphi}=r\varepsilon_{\varphi\varphi}=\csc\theta u_{\varphi,\varphi}+u_r+u_\theta\cot\theta, \quad 2S_{r\theta}=2r\varepsilon_{r\theta}=u_{r,\theta}+ru_{\theta,r}-u_\theta, \\ 2S_{r\varphi}=2r\varepsilon_{r\varphi}=\csc\theta u_{r,\varphi}+ru_{\varphi,r}-u_\varphi, \quad 2S_{\theta\varphi}=2r\varepsilon_{\theta\varphi}=\csc\theta u_{\theta,\varphi}+u_{\varphi,\theta}-u_\varphi\cot\theta. \end{gathered} \tag{2}$$

Denoting the density of the material by ρ, which is assumed to be an arbitrary function of r, the equations of motion become

$$\begin{gathered} r\Sigma_{r\theta,r}+\csc\theta\Sigma_{\varphi\theta,\varphi}+\Sigma_{\theta\theta,\theta}+2\Sigma_{r\theta}+(\Sigma_{\theta\theta}-\Sigma_{\varphi\varphi})\cot\theta=\rho r^2\ddot{u}_\theta, \\ r\Sigma_{r\varphi,r}+\csc\theta\Sigma_{\varphi\varphi,\varphi}+\Sigma_{\theta\varphi,\theta}+2\Sigma_{r\varphi}+2\Sigma_{\theta\varphi}\cot\theta=\rho r^2\ddot{u}_\varphi, \\ r\Sigma_{rr,r}+\csc\theta\Sigma_{r\varphi,\varphi}+\Sigma_{r\theta,\theta}+\Sigma_{rr}-\Sigma_{\theta\theta}-\Sigma_{\varphi\varphi}+\Sigma_{r\theta}\cot\theta=\rho r^2\ddot{u}_r. \end{gathered} \tag{3}$$

The charge equation of electrostatics is given by

$$r\Lambda_{r,r}+\Lambda_r+\csc\theta(\Lambda_\theta\sin\theta)_{,\theta}+\csc\theta\Lambda_{\varphi,\varphi}=0. \tag{4}$$

The Chen functions F, G and w, and stress functions Σ_1 and Σ_2 defined as

$$\begin{gathered} u_\theta=-\csc\theta F_{,\varphi}-G_{,\theta}, \quad u_\varphi=F_{,\theta}-\csc\theta G_{,\varphi}, \quad u_r=w, \\ \Sigma_{r\theta}=-\csc\theta\Sigma_{1,\varphi}-\Sigma_{2,\theta}, \quad \Sigma_{r\varphi}=\Sigma_{1,\theta}-\csc\theta\Sigma_{2,\varphi}. \end{gathered}$$

are used in order to simplify equations (1)-(4). Therefore, these equations can be separated into two independent sets of equations

$$rA_{,r}=MA, \tag{5}$$

and

$$rB_{,r}=PB, \ , B=[\Sigma_{rr},\Sigma_2,G,w,\Lambda_r,\phi]^T, \tag{6}$$

where

$$M=\begin{bmatrix} -2 & -C_{66}(\nabla^2+2)+r^2\rho\dfrac{\partial^2}{\partial t^2} \\ C_{44}^{-1} & 1 \end{bmatrix}, \quad \nabla^2=\frac{\partial^2}{\partial\theta^2}+\cot\theta\frac{\partial}{\partial\theta}+\csc^2\theta\frac{\partial^2}{\partial\varphi^2}.$$

It should be noted that equation (5) is related to two state variables, namely $A=[\Sigma_1,F]^T$, while equations (6) are related to the following six state variables $B=[\Sigma_{rr},\Sigma_2,G,w,\Lambda_r,\phi]^T$.

The nonzero components of the matrix P are given by

$$P_{11}=2\beta-1, \ P_{12}=\nabla^2, \ \ P_{13}=k_1\nabla^2, \ P_{14}=-2k_1+r^2\rho\frac{\partial^2}{\partial t^2},$$

$$P_{15} = 2P_{25} = -P_{64} = 2\gamma,\ P_{21} = \beta,\ P_{22} = -2,\ P_{23} = k_2\nabla^2 - 2C_{66} + r^2\rho\frac{\partial^2}{\partial t^2},$$

$$P_{24} = -k_1,\ P_{32} = C_{44}^{-1},\ P_{33} = P_{34} = -P_{55} = 1,\ P_{36} = C_{44}^{-1}f_{15},\ P_{41} = \alpha^{-1}\zeta_{33},\ P_{43} = \beta\nabla^2,$$

$$P_{44} = -2\beta,\ P_{45} = \alpha^{-1}f_{33},\ P_{52} = C_{44}^{-2}f_{15}\nabla^2,\ P_{56} = k_3\nabla^2,\ P_{61} = \alpha^{-1}f_{33},\ P_{63} = \gamma\nabla^2,$$

$$P_{65} = -\alpha^{-1}C_{33},$$

where

$$\alpha = C_{33}\zeta_{33} + f_{33}^2,\ \beta = \alpha^{-1}(C_{13}\zeta_{33} + f_{31}f_{33}),\ \gamma = \alpha^{-1}(C_{13}f_{33} - C_{33}f_{31}),$$

$$k_1 = 2(C_{13}\beta + f_{31}\gamma) - (C_{11} + C_{12}),\ k_2 = 0.5k_1 - C_{66},\ k_3 = \zeta_{11} + f_{15}^2C_{44}^{-1}.$$

Consider now two piezoceramic hollow spheres with the ratio of the inner and outer radii ξ_0. Two laws represent the functionally graded property of the material. The first one is the Reddy law [21-23] given by

$$M = M_p\mu^{\lambda} + M_z(1-\mu^{\lambda}), \tag{7}$$

where μ is the gradient index [26], M_p and M_z are material constants of two materials, namely PZT-4 and ZnO [27, 28]. The case $\mu = 0$ corresponds to a homogeneous PZT-4 hollow sphere and $\mu \to \infty$, to a homogeneous ZnO hollow sphere. The second law is expressed as

$$M = M_p\cos\mu + M_z(1-\cos\mu). \tag{8}$$

The constitutive equations for epoxy-resin material are given by

$$t_{ij} = \lambda^e\varepsilon_{kk}\delta_{ij} + 2\mu^e\varepsilon_{ij} + A^e\varepsilon_{il}\varepsilon_{jl} + 3B^e\varepsilon_{kk}\varepsilon_{ij} + C^e\varepsilon_{kk}^2\delta_{ij}, \tag{9}$$

where t_{ij} is the stress tensor, ε_{ij} is the strain tensor, λ^e and μ^e are the Lamé elastic constants, and A^e, B^e and C^e are the second-order elastic constants. The motion equations can be recast as

$$\rho^e\ddot{u}_i = t_{ij.j}, \tag{10}$$

where ρ^e is density of the epoxy material and u is the displacement vector.

At the interfaces between the hollow spheres and the matrix, the evanescent Bloch boundary conditions are introduced. Usually, at the interfaces between the scatterers and the matrix, sharp periodic boundary conditions for the displacement and traction vectors are added [3, 20].

The Bloch theorem is described by [24]

$$u(x,t) = \tilde{u}(x)\exp(\mathrm{i}kx)\exp(-\mathrm{i}\omega t),$$

$$u(x,t) = \sum_G \overline{u}_G\exp(\mathrm{iG}x)\,\mathrm{xp}(\mathrm{ik}x)\exp(-\mathrm{i}\omega t), \tag{11}$$

where x is the position, k the complex wave vector, ω the forcing frequency , t the time, u the displacement, $\tilde{u}$ the periodic wave function describing the displacement, $\bar{u}$ the magnitude of the wave, G the reciprocal lattice constants. The Bloch theorem is applied to the displacement functions at the boundaries between the scatterers and the matrix, following equation

$$U_n = U_{n+N} \exp(N(\mathrm{i}ka)\,, \tag{12}$$

where U is the wave function, a the diameter of the hollow sphere, that is a vector describing the lengths of the unit cell, the subscript n is the scatterer number and N is the number of scatterers adjacent to scatterer n. The material damping is introduced by using the complex modulus defined by

$$E_r = E(1+\mathrm{i}\eta)\,, \tag{13}$$

where E_r is the effective Young's modulus. The displacements are registered at both sides of the plate. The damping coefficient η is obtained from the ratio of the displacements at the receiver and at the input transducer. It takes some time until the oscillations become stationary. Therefore, we calculate, for each frequency, about 20 periods of the transmitted wave.

3. Inverse problem

We express the state variables of the problem (1)-(13) in the form [3]

$$\Sigma_1 = bC_{44}^0 \sum_{k=1}^{n} \mathrm{cn}^2(\xi_{k1}; m_k) + \frac{\sum_{k=0}^{n} \beta_{k1} \mathrm{cn}^2(\xi_{k1}; m_k)}{1+\sum_{k=0}^{n} \gamma_{k1} \mathrm{cn}^2(\xi_{k1}; m_k)}\,,\ \xi_{k1} = \Sigma_{11k}\xi + \Sigma_{12k}\theta + \Sigma_{13k}\varphi - \omega t\,, \tag{14}$$

$$F = b\sum_{k=1}^{n} \mathrm{cn}^2(\xi_{k2}; m_k) + \frac{\sum_{k=0}^{n} \beta_{k2} \mathrm{cn}^2(\xi_{k2}; m_k)}{1+\sum_{k=0}^{n} \gamma_{k2} \mathrm{cn}^2(\xi_{k2}; m_k)}\,,\ \xi_{k2} = F_{1k}\xi + F_{2k}\theta + F_{3k}\varphi - \omega t\,, \tag{15}$$

$$\Sigma_{rr} = bC_{44}^0 \sum_{k=1}^{n} \mathrm{cn}^2(\xi_{k3}; m_k) + \frac{\sum_{k=0}^{n} \beta_{k3} \mathrm{cn}^2(\xi_{k3}; m_k)}{1+\sum_{k=0}^{n} \gamma_{k3} \mathrm{cn}^2(\xi_{k3}; m_k)}\,,\ \xi_{k3} = \Sigma_{r1k}\xi + \Sigma_{r2k}\theta + \Sigma_{r3k}\varphi - \omega t\,, \tag{16}$$

$$\Sigma_2 = bC_{44}^0 \sum_{k=1}^{n} \mathrm{cn}^2(\xi_{k4}; m_k) + \frac{\sum_{k=0}^{n} \beta_{k3} \mathrm{cn}^2(\xi_{k4}; m_k)}{1 + \sum_{k=0}^{n} \gamma_{k3} \mathrm{cn}^2(\xi_{k4}; m_k)}, \quad \xi_{k4} = \Sigma_{21k}\xi + \Sigma_{22k}\theta + \Sigma_{23k}\varphi - \omega t, \tag{17}$$

$$G = b \sum_{k=1}^{n} \mathrm{cn}^2(\xi_{k5}; m_k) + \frac{\sum_{k=0}^{n} \beta_{k3} \mathrm{cn}^2(\xi_{k5}; m_k)}{1 + \sum_{k=0}^{n} \gamma_{k3} \mathrm{cn}^2(\xi_{k5}; m_k)}, \quad \xi_{k5} = G_{1k}\xi + G_{2k}\theta + G_{3k}\varphi - \omega t, \tag{18}$$

$$w = b \sum_{k=1}^{n} \mathrm{cn}^2(\xi_{k6}; m_k) + \frac{\sum_{k=0}^{n} \beta_{k6} \mathrm{cn}^2(\xi_{k6}; m_k)}{1 + \sum_{k=0}^{n} \gamma_{k6} \mathrm{cn}^2(\xi_{k6}; m_k)}, \quad \xi_{k6} = w_{1k}\xi + w_{2k}\theta + w_{3k}\varphi - \omega t, \tag{19}$$

$$\Lambda_r = bf_{33}^0 \sum_{k=1}^{n} \mathrm{cn}^2(\xi_{k7}; m_k) + \frac{\sum_{k=0}^{n} \beta_{k7} \mathrm{cn}^2(\xi_{k7}; m_k)}{1 + \sum_{k=0}^{n} \gamma_{k7} \mathrm{cn}^2(\xi_{k7}; m_k)}, \quad \xi_{k7} = \Lambda_{1k}\xi + \Lambda_{2k}\theta + \Lambda_{3k}\varphi - \omega t, \tag{20}$$

$$\phi = \frac{bf_{33}^0}{\zeta_{33}^0} \sum_{k=1}^{n} \mathrm{cn}^2(\xi_{k8}; m_k) + \frac{\sum_{k=0}^{n} \beta_{k8} \mathrm{cn}^2(\xi_{k8}; m_k)}{1 + \sum_{k=0}^{n} \gamma_{k8} \mathrm{cn}^2(\xi_{k8}; m_k)}, \quad \xi_{k8} = \phi_{1k}\xi + \phi_{2k}\theta + \phi_{3k}\varphi - \omega t, \tag{21}$$

where $\xi = 2r/a$, ω is the circular frequency, $C_{44}^0 = C_{44}|_{2r=a}$, $f_{33}^0 = f_{33}|_{2r=a}$, $\zeta_{33}^0 = \zeta_{33}|_{2r=a}$. The unknowns $V_m = \{\Sigma_{11k}, \Sigma_{12k}, \Sigma_{13k}, ..., \phi_{1k}, \phi_{2k}, \phi_{3k}\}$, $m = 24n$, are determined from a genetic algorithm. The goal of the genetic algorithm is to determine the set V_m, $m = 24n$ from the minimization of the residuals

$$rA_{j,r} - M_{ij}A_j = R_i, \; i, j = 1,2, \quad rB_{l,r} - P_{kl}B_l = R_k, \; k, l = 1,2,...,6. \tag{22}$$

These residuals evaluate the verification of the motion equations. The fitness function is expressed as

$$F(V_m) = \sum_{j=1}^{8} R_j^2 + \delta^2, \tag{23}$$

where δ is a measure of fitting the boundary conditions. We use a binary vector with m genes representing the real values of V_m, $m = 24n$. The length of the vector depends on the required precision, which in this case is of order $O(10^{-6})$.

The domain of the parameters $V_m \in [-a_j, a_j]$ with length $2a_j$ is divided into at least 15000 segments of the same length. That means that each parameter V_m, $m = 24n$, is represented by a string of 22 bits ($2^{21} < 3000000 \le 2^{22}$). One individual consists of the row of $24n$ genes, that is, a binary vector with $22 \times 24n$ components

$$(b_{21}^{(1)} b_{20}^{(1)} ... b_0^{(1)} b_{21}^{(2)} b_{20}^{(2)} ... b_0^{(2)} ... b_{21}^{(24n)} b_{20}^{(24n)} ... b_0^{(24n)}).$$

The mapping from this binary string into $24n$ real numbers in the range $[-a_j, a_j]$ is realized in two steps:

1. Convert each string ($b_{21}^{(j)} b_{20}^{(j)} ... b_0^{(j)}$) from the base 2 to base 10
$$(b_{21}^{(j)} b_{20}^{(j)} ... b_0^{(j)})_2 = b'_j \ , \ j = 1, 2, ..., 24n ;$$
2. Find a corresponding real number b_j, $j = 1, 2, ..., 24n$.

The genetic algorithm is linked to the problem to be solved through the fitness function (23), which measures how well an individual satisfies the requirements. From one generation to the next one, the genetic algorithm usually decreases the fitness function of the best model and the average fitness of the population. The starting population (with K individuals) is usually randomly generated. Then, new descendant populations are iteratively created, with the goal of an overall fitness function decrease from one generation to the next one.

4. Main results

Using in the inverse problem the Bloch boundary conditions greatly reduces the computational effort because they cancel the necessity to introduce non-reflecting boundary condition at the ends of the plate.

We have compares different boundary conditions, i.e. sharp periodic boundary conditions for the displacement and traction and the Bloch boundary conditions between the scatterers and the matrix to test the effectiveness of non-reflecting boundary conditions at the ends of the plate. We introduce two simple porous absorbing layers with the flow resistivity σ_e at $x_1 = 0$ and $x_1 = l$. The flow resistivity of the absorbing layers has a significant role in the modeling and stability of the computational scheme. The appropriate selection of the absorbing coefficient is necessary not only to achieve no reflections, but also to have a stable algorithm. It is easy to observe that reflection is reduced when resistivity is high, but the thickness of the absorbing layer can be small since the wave is quickly damped inside a high resistivity layer. When the resistivity is low, the reflection can also be reduced, but the thickness of the absorbing layer has to be large in order to damp the wave inside the absorbing layer. Otherwise, the remaining wave can reflect at the end of the absorbing layer and still propagates back to the medium domain. The selection of the values σ_e is made in order to accommodate the requirement of reducing unphysical reflections from the boundaries of the plate with a reasonable absorbing-layer thickness.

Our results certify the unnecessary non-reflecting boundary condition at the ends of the plate, if Bloch boundary conditions between the scatterers and the matrix are used. The stability of the genetic algorithm is more than satisfactory. The time required for calculations of the response functions and dispersion curves is very short compared to the time needed if the sharp periodic boundary conditions between the scatterers and the matrix and non-reflecting boundary condition at the ends of the plate are used.

The response functions and dispersion curves are calculated by using the cnoidal method [30]. The frequency response functions for longitudinal displacement in direction Ox_1, and transverse displacement in direction Ox_2, respectively, with /without damping is presented in Fig. 2 in the case of the Reddy law (7). The case of cosine law (8) is presented in Fig. 3. The amplitude is dimensionless U/U_0 with U_0 a reference value. We see from both case that the damping reduces the amplitudes of vibrations for both waves.

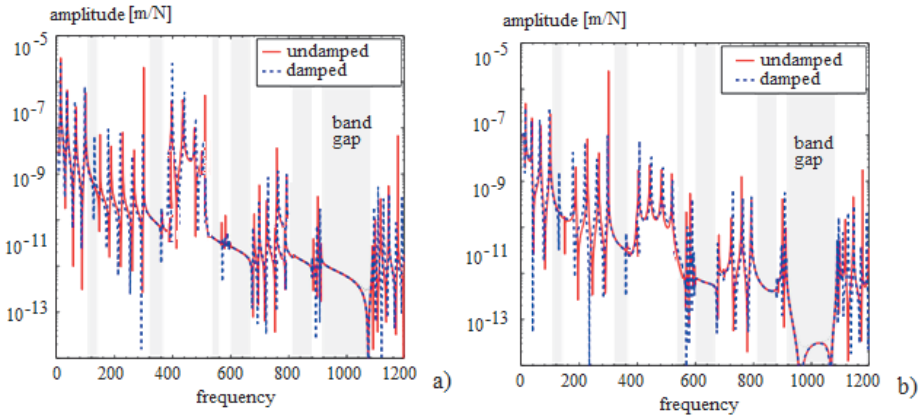

Fig. 2. Frequency response functions for a) longitudinal displacement in direction Ox_1, and b) transverse displacement in direction Ox_2, with /without damping, in the case of Reddy law.

The dispersion curves are presented in Figs. 4 and 5, for both the longitudinal Ox_1 and transverse Ox_2 directions, respectively, without and with material damping. Red lines denote the undamped case while blue square lines denote the damped case. The band gaps are highlighted in grey. Fig. 4 displays the dispersion curves in the longitudinal direction: (a) real part and (b) imaginary part, and Fig. 5, the dispersion curves in the transverse direction: (a) real part and (b) imaginary part.

The band gaps are determined from the dispersion curves. The band gaps are regions of frequencies for which the imaginary parts of all wave vectors are non-zero. The imaginary parts of the wave vectors represent the attenuation of waves and a non-zero value of the imaginary part means that the wave is reducing in amplitude after reflection. A positive imaginary part is considered to be an attenuating wave in the reverse direction. The band gaps are highlighted n Figs. 5

and 6. For the band gaps with complex wave vectors, the waves propagate through the medium but the magnitude of the waves decreases with increasing distance.

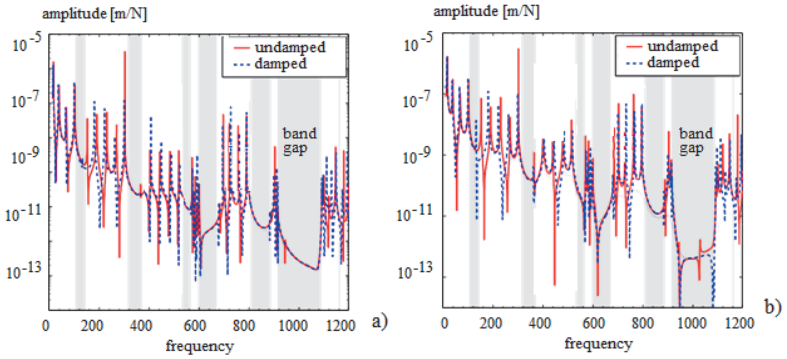

Fig. 3. Frequency response functions for a) longitudinal displacement in direction Ox_1, and b) transverse displacement in direction Ox_2, with /without damping, in the case of cosine law.

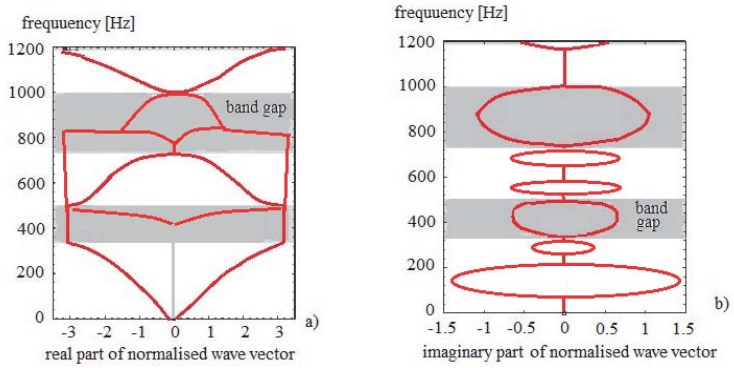

Fig. 4. Dispersion curves for longitudinal direction: (a) real part and (b) imaginary part.

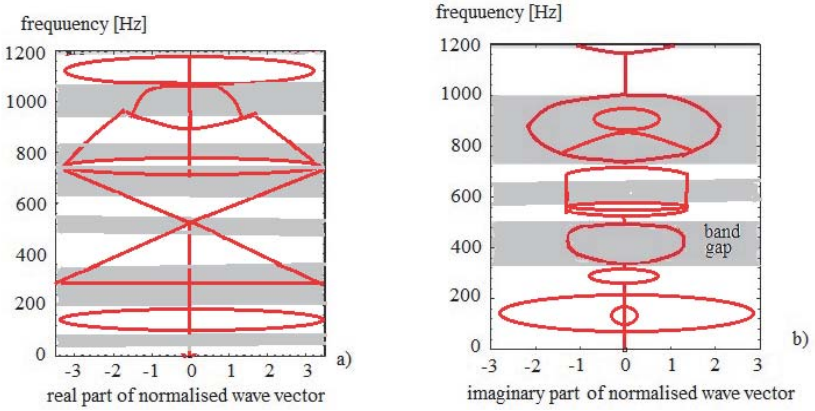

Fig. 5. Dispersion curves for transverse direction: (a) real part and (b) imaginary part.

5. Concluding remarks

An inverse problem based on Bloch wave boundary conditions and the nonlinear superposition of waves is proposed in this paper in order to calculate the band structure of a sonic plate. The sonic plate is composed of an array of acoustic scatterers which are piezoceramic hollow spheres embedded in an epoxy matrix. The scatterers are made from functionally graded materials with radial polarization, which support the Reddy and cosine laws. Using the Bloch boundary conditions greatly reduces the computational effort because they cancel the necessity of introducing the non-reflecting boundary condition at the ends of the plate. We have compares different boundary conditions, i.e. sharp periodic boundary conditions for the displacement and traction and the Bloch boundary conditions between the scatterers and the matrix to test the effectiveness of non-reflecting boundary conditions at the ends of the plate. Our results certify the lack of importance of the non-reflecting boundary condition at the ends of the plate, if Bloch boundary conditions are used.

The cnoidal method is applied to determine the band structure of sonic periodic structures using only the responses at different points without knowledge of the material properties. Using the nonlinear superposition principle and the Bloch wave boundary conditions, the relationship between the displacements at adjacent scattereres was determined. The stability of the genetic algorithm is more than satisfactory. Time required for calculations of the response functions and dispersion curves is very short compared to the time needed if the sharp periodic boundary conditions between the scatterers and the matrix and non-reflecting boundary condition at the ends of the plate are used.

References

[1] Miyashita, T., Taniguchi, R., Sakamoto, H., *Experimental full band-gap of a sonic-crystal slab structure of a 2D lattice of aluminum rods in air*, Proc. 5th World Congress on Ultrasonics TO-PM04.02, 2003.

[2] Miyashita, T., *Full band gaps of sonic crystals made of acrylic cylinders in air-numerical and experimental investigations*, Jpn. J. Appl. Phys. 41, 3170-1-3175, 2002.

[3] Munteanu, L., Chiroiu, V., *On the dynamics of locally resonant sonic composites*, European Journal of Mechanics-A/Solids, 29(5), 871–878, 2010.

[4] Chiroiu, V., Brişan, C., Popescu, M.A., Girip, I., Munteanu, L., *On the sonic composites without/with defect*, Journal of Applied Physics, vol. 114 (16), pp. 164909-1-10, 2013.

[5] Munteanu, L., Chiroiu, V., Donescu, St., Brişan, C., *A new class of sonic composites*, Journal of Applied Physics, 115, 104904, 2014.

[6] Girip, I., Munteanu, L., *Modeling of non-stationary vibration signals based on the modified Kronecker sequences*, PAMM- Proceedings in Applied Mathematics and Mechanics, vol. 15, iss 1, 195-196, work presented to 86th Annual Meeting of GAMM hosted by Università del Salento March 23-27, 2015.

[7] Girip, I., *On the acoustics of sonic composites*, PAMM- Proceedings in Applied Mathematics and Mechanics, Gesellschaft für Angewandte Mathematik und Mechanik (GAMM) ISSN: 1617-7061, vol. 16, issue 1, 2016.

[8] Joannopoulus, J.D., Johnson, S.G., Winn, J.N., Meade, R.D., *Photonic Crystals, Molding the Flow of Light* (princeton University Press 2008).

[9] Goffaux, C. and Sanchez-Dehesa, J., *Two-dimensional phononic crystals studied using a variational method: application to lattices of locally resonant materials*, Phys. Rev. B **67,** 144301, 2003.
[10] Goffaux, C., Maseri, F., Vasseur, J. O., Djafari-Rouhani, B. and **Lambin**, P., *Measurements and calculations of the sound attenuation by a phononic band gap structure suitable for an insulating partition application*, Appl. Phys. Lett., **83,** 281–283, 2003.
[11] Gupta, B. C. and Ye, Z., *Theoretical analysis of the focusing of acoustic waves by two-dimensional sonic crystals*, Phys. Rev., E **67** 036603, 2003.
[12] Munteanu, L., Chiroiu, V., Serban, V., *From geometric transformations to auxetic materials*, CMC: *Computers, Materials & Continua*, 2014**.**
[13] Rubio, C., Caballero, D., Sánchez-Pérez, J.V., Martínez-Sala, R., Sánchez-Dehesa, J., Meseguer, F., Cervera, F., *The existence of full gaps and deaf bands in two-dimensional sonic crystals*, J. Lightwave Technol., 17, 11, 2202–2207, 1999
[14] Sáchez-Pérez, J.V., Caballero, D., Martínez-Sala, R., Rubio, C., Sánchez-Dehesa, J., Meseguer, F., Llinares, F., Gálvez, F., et al., *Sound attenuation by a two-dimensional array of rigid cylinders*, Phys. Rev. Lett., 80, 24, 5325–5328, 1998.
[15] Vasseur, J.O., Deymier, P.A., Khelif, A., Lambin, P., Djafari- Rouhani, B., Akjouj, A., Dobrzynski, L., Fettouhi, N., Zemmouri, J., *Phononic crystal with low filling fraction and absolute acoustic band gap in the audible frequency range: A theoretical and experimental study*, Phys. Rev. E 65, 056608–056614, 2002.
[16] Kafesaki, M., Economou, E.N., *Interpretation of the bandstructure results for elastic and acoustic waves by analogy with the LCAO approach*, Phys. Rev. B 52, 18, 13317–13331, 1995.
[17] Psarobas, I.E., Stefanou, N., Modinos, A., *Scattering of elastic waves by periodic arrays of spherical bodies*, Phys. Rev. B 62, 1, 278–291, 2000.
[18] Martínez-Sala, R., Sancho, J., J.V. Sánchez, V. Gómez, J. Llinares, F. Meseguer, *Sound attenuation by sculpture*, Nature, 378 241, 1995.
[19] Liu, Z., Zhang, X., Mao, Y., Zhu, Y.Y., Yang, Z., Chan, C.T., Sheng, P., *Locally resonant sonic materials*, Science, 289, 1734–1736, 2000.
[20] Hirsekorn, M., Delsanto, P.P., Batra, N.K., Matic, P., *Modelling and simulation of acoustic wave propagation in locally resonant sonic materials*, Ultrasonics, 42, 231–235, 2004.
[21] Reddy, J.N., *A Generalization of Two-Dimensional Theories of Laminated Composite Laminate*, Comm. Appl. Numer. Meth., 3, 173–180, 1987.
[22] Reddy, J.N., Liu, C.F., *A higher-order theory for geometrically nonlinear analysis of composite laminates*, NASA Contractor Report 4056, 1987.
[23] Reddy, J.N., Wang, C.M., Kitipornchai, S., *Axisymmetric bending of functionally graded circular and annular plates*, Eur. J. Mech., A/Solids 18, 185–199, 1999.
[24] Junyi, L., Balint, D.S., *An inverse method to determine the dispersion curves of periodic structures based on wave superposition*, J. of Sound and Vibration, 350, 41-72, 2015.
[25] Chiroiu, V., Munteanu, L., *On the free vibrations of a piezoceramic hollow sphere*, Mech. Res. Comm., Elsevier, 34, 2, 123–129, 2007.
[26] Chen, W. Q, Wang, L.Z, Lu, Y., *Free vibrations of functionally graded piezoceramic hollow spheres with radial polarization*, J. Sound Vibr., 251, 1, 103–114, 2002.
[27] Chen, W.Q., *Vibration theory of non-homogeneous, spherically isotropic piezoelastic bodies*, J. Sound Vibr., 229, 833–860, 2000.
[28] Tang, Y.Y., Xu. K., *Exact solutions of piezoelectric materials with moving screw and edge dislocation*, Int. J. Eng. Sci. 32, 1579–1591, 1994.
[29] Gei, M., *Elastic waves guided by a material interface*, European Journal of mechanics-A/Solids, 27, 3, 328–345, 2008.
[30] Munteanu, L., Donescu, St., *Introduction to Soliton Theory: Applications to Mechanics*, Book Series "Fundamental Theories of Physics", vol.143, Kluwer Academic Publishers, 2004.